



Experimental investigation of effects of variation in heating rate, temperature and heat flux on fire properties of a non-charring polymer

Ariza S. Abu-Bakar¹ · Marlene J. Cran³ · Khalid A. M. Moinuddin^{2,3}

Received: 30 November 2017 / Accepted: 18 November 2018 / Published online: 3 December 2018
© Akadémiai Kiadó, Budapest, Hungary 2018

Abstract

During fire, charring and non-charring polymers undergo reactions in the solid phase (pyrolysis) and in the gas phase (combustion). These reactions can be modelled using computational fluid dynamics-based fire modelling for the prediction of fire growth and spread. Given that many fire properties vary with temperature including heating rate and radiation flux, improvements in fire simulations can be made by accounting for these variations. This study characterizes the fire properties of the non-charring synthetic polymer poly(methyl methacrylate) (PMMA) for coupled pyrolysis and combustion simulation. Under pyrolysis, the heat of reaction of PMMA varies with heating rate due the change in residence time facilitating volatilization at any given temperature, particularly at higher heating rates. As a result, the volatiles are formed when the sample has reached higher temperature and therefore more heat flow is needed to assist this process at higher heating rates. Similarly, combustion parameters are also found to vary with the incident radiation flux; however, the variation is relatively minimal. In this study, thermal conductivity and specific heat capacity did not vary with temperature for PMMA.

Keywords Pyrolysis · Combustion · Chemical kinetics · Heat of reaction · Heating rate · Effective heat of combustion

List of symbols

A	Pre-exponential factor, s^{-1}	\dot{m}''	Mass loss rate per unit area, $kg\ m^{-2}\ s^{-1}$
A'	Area under the peak, m^2	n	Reaction order
A_T	Area under the curve, m^2	\dot{q}''_c	Convective heat flux, $kW\ m^{-2}$
C_p	Specific heat capacity, $J\ kg^{-1}\ ^\circ C^{-1}$	\dot{q}''_r	Radiative heat flux, $kW\ m^{-2}$
E_a	Activation energy, $kJ\ min^{-1}$	R	Universal gas constant, $J\ kg^{-1}\ mol^{-1}\ K^{-1}$
EHoC	Effective heat of combustion, $kJ\ kg^{-1}$	SEA	Specific extinction area, $m^2\ kg^{-1}$
HoR	Heat of reaction, $kJ\ kg^{-1}$	s	Solid
HRR	Heat release rate, kW	T	Temperature, $^\circ C$ or K
k	Conductivity, $W\ m^{-1}\ ^\circ C^{-1}$	T_1	Peak 1 integration temperature, $^\circ C$
MLR	Mass loss rate, $m^2\ kg^{-1}$	T_2	Peak 2 integration temperature, $^\circ C$
MC	Moisture content, %	t	Time, s
m_i	Sample mass at the approximation	x_i	Mass loss fraction
		Y	Weight fraction of conversion
		y_i	Fraction of i th gaseous products yield
		dY/dT	Pyrolysis rate
		dt/dT	Heating rate
		w	Instantaneous sample mass, mg
		w_i	Initial sample mass, mg
		w_f	Final sample mass, mg
		w_{fc}	Final sample mass (cone), mg
		w_{ic}	Initial sample mass (cone), mg
		β	dT/dt or heating rate, $K\ s^{-1}$

✉ Khalid A. M. Moinuddin
khalid.moinuddin@vu.edu.au

¹ School of Housing, Building and Planning, Universiti Sains Malaysia, 11800 George Town, Penang, Malaysia

² Centre for Environmental Safety and Risk Engineering, Victoria University, Melbourne, Australia

³ Institute for Sustainable Industries and Liveable Cities, Victoria University, Melbourne, Australia

ΔE	Heat flow into DSC sample, mW
ΔH_{DSC}	Normalized enthalpy, kJ kg^{-1}
ΔH	Heat of reaction, kJ kg^{-1}
ΔH_{R}	Heat of reaction in fire model, kJ kg^{-1}
ΔH_{con}	Normalized HoR, kJ kg^{-1}
ΔH_{enh}	Enhanced HoR, kJ kg^{-1}
ρ	Density, kg m^{-3}
v_s	Yield of solid residue, %

Introduction

Fire scenarios involve pyrolysis process where material decomposition occurs as a result of the release of gases and other volatiles, and combustion process which is an exothermic gas phase reaction between gaseous fuel and oxygen. State-of-the-art numerical simulation (computational fluid dynamics, CFD, based) of fire scenarios includes coupled pyrolysis-combustion modelling [1]. This kind of numerical simulation of coupled solid- and gas-phase reactions requires a set of thermo-physical properties, chemical kinetics and combustion parameter data. These can be collectively termed as “fire properties”. Most of these are macroscopic or bulk effective model parameters, rather than microscopic or fundamental properties. A number of them are nominally constant (such as density and emissivity) while others vary (such as specific heat capacity and conductivity) with respect to temperature, heating rate, incident radiation, etc. As the model output is strongly dependent on these fire properties, characterization of these properties is vital.

The size of a growing fire changes with time and so the temperature of materials (both combustible and non-combustible), the rate at which the materials are heated, and the incident radiation upon the materials also changes. Many thermal events such as evaporation, crystallization and decomposition are kinetic in nature, i.e. functions of both time and temperature. Therefore, these events will occur at different temperatures when the material is heated at a different rate. Thermogravimetric analysis (TGA) and differential scanning calorimetry (DSC) are often used to determine parameters (activation energy, E_a , pre-exponential factor, A , reaction order, n , char yield and heat of reaction, HoR) related to pyrolysis reactions. Previous studies reporting TGA data show that pyrolysis decomposition is shifted to a higher temperature range when materials are heated at higher rates [2–6]. It should be noted that with the exception of one study [5], most of these studies are limited to heating rates of 50 K min^{-1} , whereas during fire, materials can be heated at rates of

200 K min^{-1} or greater [5]. Starink and Gregson [7] presented DSC curves of aluminium-based alloys at varying heating rates, and similar to TGA measurements, the DSC data showed that various thermal events are shifted to higher temperatures when the alloys were heated at higher heating rates.

The characterization of the combustion parameters for simple homogeneous materials requires a detailed evaluation such as: (1) the chemical composition of the combustible material through ultimate analysis; (2) the yield of basic combustion products (i.e. CO , CO_2 , soot and char) and the effective heat of combustion (EHoC) via cone calorimetry [8, 9]. In recent years, microscale combustion calorimetry (MCC) has also been used to characterize combustion parameters [10, 11]. However, for large-scale flame spread modelling, characterization using cone calorimetry is more conventional. Several thermal properties influence a rise in temperature of a material when it is exposed to heat including thermal conductivity (k) and specific heat capacity (C_p). Thus, it is important to understand how properties change with various fire conditions and how they can be quantified to be used for fire simulations. This study aims to demonstrate that there is a need to develop methods to characterize fire properties for unknown, new or novel materials using PMMA as a model non-charring polymer. The values of k and C_p are also the focus of this study as they are important inputs required in fire simulations [12].

Experimental

Theoretical background

Determination of the kinetic triplet

When a combustible material is heated, its molecules collide with each other, resulting the generation of kinetic energy. Once the kinetic energy is greater than the minimum energy threshold, a chemical reaction occurs and in the case of pyrolysis, material decomposition and release of volatiles occur. The pre-exponential factor, A (1 s^{-1}), also known as a frequency factor, is the frequency of the collisions between molecules and the activation energy, E_a (kJ min^{-1}) is the minimum energy requirement that must be met for a kinetic reaction to occur. At elevated temperatures, more collision of molecules occurs which speeds up kinetics. The reaction order, n , is the index or exponent to which the concentration term in the chemical reaction rate equation (Eq. 1) is raised. These three parameters are often termed as the chemical kinetic triplet.

It is often assumed that the pyrolysis reactions take place as per the Arrhenius equation:

$$\frac{dY}{dT} = \frac{A}{\beta} e^{-\frac{E_a}{RT}} (1 - Y)^n \tag{1}$$

where Y is the fraction of conversion from solid to gas, dY/dT is the pyrolysis rate, β is the heating rate, T is the sample temperature, and R is the universal gas constant. The value of Y is determined by:

$$Y = \frac{w - w_f}{w_i - w_f} \tag{2}$$

where w is the mass at a particular temperature, w_i is the initial sample mass, and w_f is the final sample mass. By applying appropriate data reduction methods on TGA data A , E_a and n can be obtained. In this study, the inflection point method [13] is chosen due to its robust ability to analyze the whole set of TGA data to determine the kinetic triplet of the sample. This method is based on the employment of a linear plot and the coefficients of the linear equation. Although other methods are available [14], the inflection point method is used in this study as it assists in showing the effect of heating rate on the values of the kinetic triplet.

Determination of thermo-physical properties

In most CFD-based fire models such as FDS [15], the one-dimensional heat transfer calculation for the solid-phase temperature $T(x,t)$, is applied in the direction x facing the solid, where the point $x = 0$ represents the surface is given by:

$$\rho_s c_s \frac{\partial T_s}{\partial T} \equiv \frac{\partial}{\partial x} \left(k_s \frac{\partial T_s}{\partial x} \right) \tag{3}$$

where k_s , ρ_s and c_s are the thermal conductivity ($\text{W m}^{-1} \text{K}^{-1}$), density (kg m^{-3}) and specific heat capacity ($\text{kJ kg}^{-1} \text{K}^{-1}$) of the solid material, respectively.

In this study, k and C_p were measured using a hot disc analyser (HDA) via the transient plane source technique with which is a non-steady-state method that allows fast, accurate measurements of thermal properties simultaneously [16]. The probing depth is one of the crucial factors in the determination of k and C_p by means of HDA where the instrument works on the assumption that the sample has sufficient depth to allow enough time for the thermal wave or thermal penetration depth over the measurement period. The probing depth should be less than the geometrical boundary of the sample so that the thermal wave should not cross the sample boundary. The post-processing software of the HDA directly provides the values of k and C_p .

The boundary condition to calculate the surface temperature of the combustible solid facing the direction of fire is given by:

$$-k_s \frac{\partial T_s}{\partial x} \equiv \dot{q}_r'' + \dot{q}_c'' - \dot{m}'' \Delta H_R \tag{4}$$

where T_s is the temperature of the solid, \dot{q}_c'' is the convective heat flux, \dot{q}_r'' is the radiative heat flux and \dot{m}'' is the volatile production rate (mass flux) obtained from Eqs. (1) and (2), and ΔH_R is the HoR or gasification (i.e. the latent heat required during the gasification of a solid fuel [17]). For relatively low (i.e. microscopic) heating rates such as those encountered using TGA experiments, a gasification process will occur via a solid–liquid–gas transformation, particularly in the case of materials that melt such as PMMA. For higher heating rates, gasification can occur via a solid–gas transformation which may require more energy. For some materials undergoing endothermic reactions, heating rates higher than 5 K min^{-1} are recommended [17] and are considered to be macroscopic heating rates. In this study, the term HoR is defined as an effective model parameter to account for heat loss during a pyrolysis process for the materials studied. Various attempts have made to use DSC to quantify the HoR for combustible materials [18–20] and a relatively new method describes a technique developed using TGA and DSC experiments for HoR determination [21]. The protocol developed and used in this study is presented in “Protocol for HoR determination” section.

Parameterization of the combustion model

The combustion process is often represented by the following stoichiometric reaction:



where the quantities ν_{Fuel} , ν_{O_2} and ν_{Products} are the stoichiometric coefficients for the overall combustion process that reacts fuel with oxygen to produce a number of products, respectively. The parameterization of the combustion model requires a detailed evaluation of properties such as: (1) the chemical composition of the combustible material through ultimate analysis; (2) the yield of basic combustion products (i.e. CO, CO₂ and soot) and the heat of combustion via cone calorimetry; and (3) the yield of other combustion products (i.e. those containing nitrogen and chlorine). The latter is more suitable for complex materials and can be measured using Fourier transform infrared (FTIR) spectroscopy [22, 23]. In the case of PMMA, the polymer is not an overly complex material with a well-characterized chemical composition and as such, techniques such as FTIR spectroscopy are not essential for its analysis. Chemically, PMMA is comprised of C (59.1%), H (7.9%) and O (31.9%) with trace amounts

of N, S, Cl and H₂O [24]. The C to O ratio, a common parameter used to characterize fuels, is 1.9.

The cone calorimeter is a bench-scale apparatus for measuring the heat release rate (HRR) of materials, among other parameters, by the principle of oxygen consumption [8]. The HRR is typically measured per unit area, \dot{q}'' (kW m⁻²). It also simultaneously measures the mass loss rate (MLR), CO yield, CO₂ yield and soot yield. The EHoC is derived from the HRR and the mass flux from pyrolysis, \dot{m}'' :

$$\text{EHoC} = \dot{q}'' / \dot{m}'' \quad (6)$$

The values of above combustion parameters are directly obtained via the post-processing software of the cone calorimeter. Char yield can be determined using the initial mass, final mass and moisture content:

$$\text{Char yield} = \frac{w_{fc}}{w_{ic}(1 - \text{MC})} \quad (7)$$

where w_{fc} and w_{ic} are the final mass and initial mass of the sample in the cone calorimeter experiment, respectively, and MC is the moisture content obtained from the TGA experiment.

Protocol for HoR determination

To obtain the HoR, a method derived from the work of Huffman and Pan [19] was used in this study. An ASTM method, E2160 [25], describes a procedure to test the specimen in DSC by heating at 10 K min⁻¹ in the temperature region where the chemical reaction is known to take place. The weight loss during the reaction is recorded by reweighing the sample after the specimen had been cooled down to ambient temperature. The HoR is then calculated by integrating the recorded heat flow versus time and the normalized HoR is calculated by dividing this value by the initial mass of the specimen. Huffman and Pan [19] observed that using initial mass in the calculations leads to inconsistencies in the results. They suggested that this practice is invalid when testing samples which undergo phase change or thermal degradation during the experiment. Thus, they compared the two methods, one which uses initial mass and another using instantaneous mass which is obtained from TGA data. Since a DSC does not have the capability to measure mass change during the experiment, the mass change data, as a function of sample temperature needs to be obtained from a TGA curve instead. It is therefore critical to maintain the same experimental conditions in both experiments in order to make relevant correlation between them.

From the DSC curve, the heat flow versus time or temperature is plotted and the area under the curve is

determined and the following two equations have been developed to determine the HoR [19]:

$$\Delta H_{\text{con}} \times w_i = KA' \quad (8)$$

$$\Delta H_{\text{enh}} = \sum \frac{KA_T}{nm_i} \quad (9)$$

where ΔH_{con} corresponds to the normalized HoR calculation using the initial mass while ΔH_{enh} takes into account the mass change throughout the experiment, w_i is the initial mass of the sample, K is the calibration coefficient and A' is the area under the peak. In Eq. (9), n is the number of approximations, m_i is the mass of the sample at that approximation, and A_T is the area under the curve within approximation segment. The calibration constant varies with the instrument used. It was concluded that the HoR value obtained using the enhanced equation is higher than that calculated using the conventional equation for an experiment involving endothermic decomposition but lower for materials that react exothermically with volatile gases. The HoR calculated using the enhanced and conventional equation is observed to be the same for materials that undergo phase transitions [19].

Hostikka [26] suggested following a method similar to that of Huffman and Pan [19] where both the initial sample masses and the heating rates are the same for both TGA and DSC measurements. The data from both instruments are matched at the same and the respective heat flows obtained from the DSC test are divided by respective un-subtracted masses obtained from TGA test. The heat flow/mass versus temperature is plotted, and the area under the curve where pyrolysis occurs is calculated to determine HoR:

$$\Delta H_R = \frac{\Delta H_{\text{DSC}} \cdot w_i \cdot y_i}{x_i w_i} = \frac{\Delta H_{\text{DSC}} \cdot y_i}{x_i} \quad (10)$$

where ΔH_R is the HoR required for Eq. (4), ΔH_{DSC} is the normalized enthalpy, y_i is the yield of gaseous products (fraction of solid fuel), and x_i is the fractional mass loss with values of y_i and x_i for non-charring materials are equal to unity. To obtain ΔH_{DSC} , the definite integral should be evaluated between the temperature ranges on which the reaction occurs:

$$\Delta H_{\text{DSC}} = \int_{T_1}^{T_2} \frac{\Delta E}{w} dT \quad (11)$$

where ΔE is the instantaneous heat flow into the sample.

An example of a DSC heat flow versus temperature curve for PMMA and the corresponding TGA mass loss versus temperature curve are presented in Fig. 1a, b, respectively. In Fig. 1c, the derived heat flow/unit mass versus temperature profile derived from the combined DSC

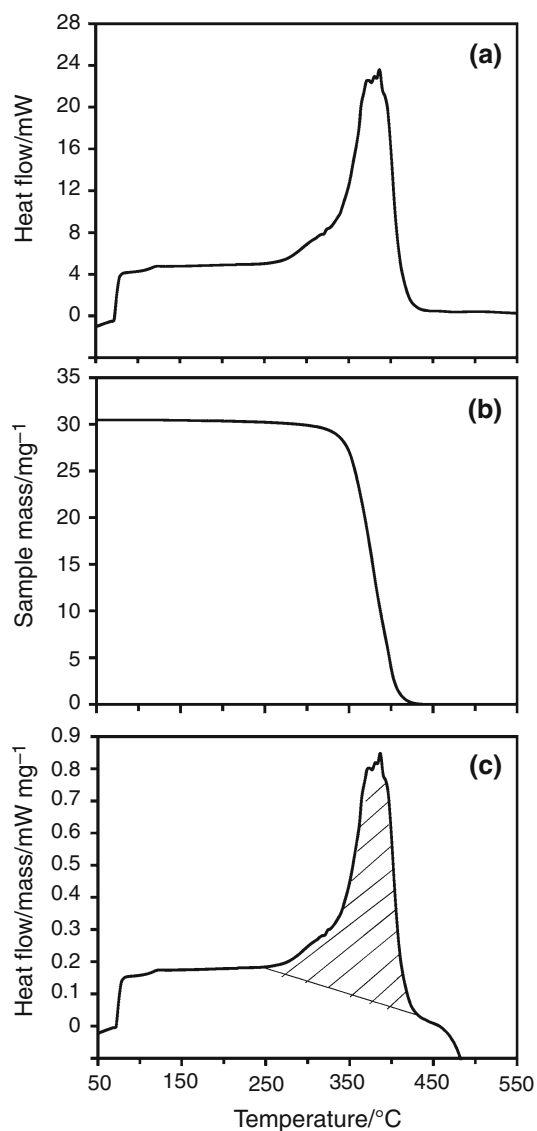


Fig. 1 HoR determination: **a** DSC heat flow curve for PMMA at 20 K min⁻¹; **b** TGA mass loss curve for PMMA at 20 K min⁻¹; and **c** calculated heat flow/mass plot at matched temperature from (a) and (b)

and TGA data is presented by matching the temperatures from the two sets of data. In this graph, the peak represents the pyrolysis of the PMMA. The temperature range over which the pyrolysis reaction occurs can be determined from the TGA curve. In Fig. 1c, the pyrolysis of PMMA occurs between 250 and 410 °C with the shaded area representing the ΔH_{DSC} which was calculated using a MATLAB program::

$$\frac{\text{heat flow (kW)}}{\text{instantaneous mass (kg)}} \times \frac{\text{pyrolysis range (}^{\circ}\text{C)}}{\text{heating rate (}^{\circ}\text{C/S)}} = \frac{\text{kJ}}{\text{kg}} \quad (12)$$

It is also possible to use different initial sample masses for TGA and DSC tests to obtain accurate HoR values by normalizing the instantaneous DSC heat flow into the sample by its initial mass. Here, a heat flow per unit of the initial sample mass (mW mg⁻¹) versus temperature profile is obtained rather than the profile shown in Fig. 1a. Similarly, the instantaneous TGA sample mass can be normalized by the initial mass resulting in a dimensionless mass fraction versus temperature rather than the profile shown in Fig. 1b. The data from both profiles are then matched, and the corresponding temperatures and the same profile as that shown in Fig. 1c can be obtained, and the ΔH_{DSC} can be obtained from this profile using Eqs. (11–12) as above.

Thermal analysis experiments

A PerkinElmer TGA7 (PTGA) and a Mettler Toledo TGA/DSC1 STARE system (MTGA) were used for the TGA experiments, and a Mettler Toledo DSC1 STARE system (MDSC) was used for the DSC experiments. Both the TGA and DSC tests were conducted under non-isothermal conditions with nitrogen flow maintained at 50 mL min⁻¹ to replicate pyrolysis conditions in the absence of air which usually occurs when there is a flaming combustion reaction preventing air from reaching the material. The PMMA sample was cut into small pieces approximately 1 × 1 mm. A 5 mg PMMA sample was used for each of PTGA and DSC experiments, and heating rates between 5 and 200 K min⁻¹ over the temperature range of 50–550 °C were employed. The nitrogen flow rate and mass sample size were based on the study of Abu-Bakar and Moinuddin [2] and Wadhvani et al. [14] who also used similar sample mass of leaf litter for different heating rates. However, the MTGA required a larger sample size of > 20 mg and therefore was only used for deriving some kinetic parameters. For the DSC measurements, 40 μL aluminium pans with pin-holed lids were used in order to enable the gases release from the crucible [21]. Matched data from the PTGA and MDSC were used for calculating HoR, and test data from the MTGA were also used to identify any difference in thermal lag between the PTGA and MDSC.

A cone calorimeter manufactured by Fire Testing Technology was used in this study for obtaining combustion parameters. For experiments, slabs of PMMA measuring 100 × 100 × 25 mm were prepared and tested from 20 to 75 kW m⁻² irradiance level. The testing procedure used in this measurement is based on ASTM E1354 [8] where the samples were wrapped with aluminium foil around the edge with the shiny part of the foil facing towards the sample and a piece of fibre blanket was placed at the bottom of the sample holder for insulation.

Values of k and C_p of PMMA were determined using Hot Disk Transient Plane Source (TPS) 500, a non-isothermal HDA, manufactured by ThermTest Inc. The PMMA samples tested for these parameters were in the same form as tested for the cone calorimeter experiment. For each measurement, a sample was placed on the specimen holder and sandwiched over the hot disk sensor and these were placed in an oven to heat the sample. Kapton sensors of type 5501 with a 6.403 mm radius and type 5465 with a 3.189 mm radius were used in this study. These sensors function as both the heat source as well as temperature sensors [12] and can be used for temperatures up to 300 °C. A hole was drilled horizontally into the sample to accommodate the thermocouple which was used to measure the temperature of the sample as a secondary measurement to confirm the values measured by the sensor.

All equipments used in this study were calibrated prior to the measurement, and samples used for all measurements were conditioned for 48 h with 50% relative humidity at 23 °C. Multiple runs were carried out for each test to obtain consistent results.

Results and discussion

Characterization of pyrolysis parameters

The PMMA DTG curves obtained at seven heating rates ranging from 5 to 200 K min⁻¹ are shown in Fig. 2a for the MTGA and Fig. 2b for the PTGA instruments. The corresponding MDSC heat flow versus temperature curves for PMMA at the matching heating rates is presented in Fig. 2c. The thermal lag of the PTGA curves were calibrated so that the peaks representing pyrolysis reactions align with the corresponding DSC curve peaks. It can be observed that the decomposition process, as indicated by the DTG peak locations, is shifted to higher temperatures as the heating rate is increased and this has been widely reported in previous studies [3, 27–34]. Moreover, the peak value is gradually reduced as the heating rate is increased.

Similar to the TGA data, the DSC data in Fig. 2b show that the peak heat flow locations for fuel release shifted towards higher temperatures as the heating rate increased. In addition, the peak value indicating the HoR generally increased at higher heating rates. Explanations for the observed decomposition shift include the decreased residence time of volatiles within cellulosic (charring) materials which results in the reaction commencing at higher temperatures [35, 36]. Moreover, at high heating rates, volatiles are more quickly formed and therefore they spend less time within the sample and this can also be applicable to non-charring materials. Milosavljevic et al. [37] suggested a “mass transport limitation” involving the

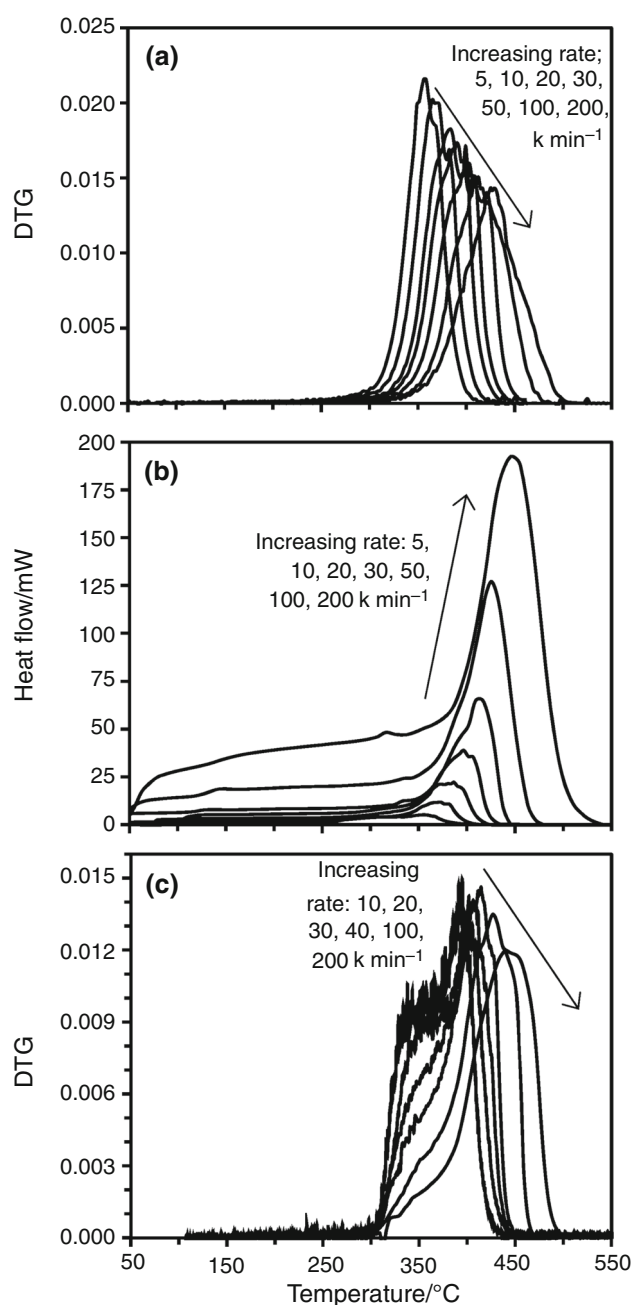


Fig. 2 Thermal data for PMMA obtained using TGA and DSC at various heating rates: **a** MTGA DTG plots; **b** MDSC curves; and **c** PTGA DTG plots

restriction of physical transport of the reactants at the gas/solid interface may also be responsible for the shift in cellulosic materials. In the present study, the sample has less residence time within the vicinity of any specific temperature at a higher heating rate and therefore, by the time the volatiles are formed, the sample reaches a higher temperature. Furthermore, a greater heat flow is needed to

assist the formation of volatiles quickly at higher heating rates.

Kinetic triplets of PMMA

In the case of PMMA, only single pyrolysis reactions are observed to take place although it is known that multiple pyrolysis reactions can occur in various combustible materials. For simplicity, however, most pyrolysis models are based on single “effective” reaction and the inflection point method is capable of determining multiple reaction kinetics as well as “effective” reaction kinetics [13]. The kinetic triplet of PMMA derived from Fig. 2a using the inflection point method is presented in Fig. 3 as a function of heating rates (dT/dt). These figures show that the value of A , E_a and n varies with dT/dt which is consistent with decomposition shift observed in Fig. 2.

The values obtained in this study are also compared in Fig. 3 with those reported in the literature. Matala [27] studied these parameters comprehensively; however, an optimization technique was used to study the kinetics for the experimental raw data [38]. In this technique, an optimization algorithm performs permutations with combinations of the values of A , E_a and n . With each set of kinetic values, simulations are then run using a pyrolysis model with values of the model that match the best with the experimental result taken as the “model-specific” values. These are not true values as they may or may not be universally applied to all models, and therefore, a different set of kinetic triplet values were obtained [27]. It is well known that there is a strong interdependence among the kinetic triplet [39, 40] and by applying two different set of triplets (one set from the current study and one set from Matala [27] to Eq. 1), the same mass loss rate was obtained which confirms this interdependence.

The values of the kinetic parameters presented in Fig. 3 lie within the range of values found in the literature. The E_a value for PMMA in the current study, $232.6 \text{ kJ min}^{-1}$, was compared with those of other workers including Ballistreri et al. [40] whose E_a value agrees well particularly at the heating rate of 5 K min^{-1} . The E_a value of Zhang [41] is also close at the heating rate of 10 K min^{-1} ; however, the value reported by Matala [27] is significantly lower than the other reported values. Han et al. [42] obtained the kinetic triplet values using two methods, namely the peak property method (PPM) and the Freeman and Carroll method (FC), and all of these values are very close to those of the present study with the exception of the A values. They obtained E_a values of 214.5 and $216.4 \text{ kJ min}^{-1}$ at 10 K min^{-1} for the PPM and FC, respectively, are lower than that obtained in the present study of $232.6 \text{ kJ min}^{-1}$. The value of n value is also close to our current study and agrees well at 20 K min^{-1} . The

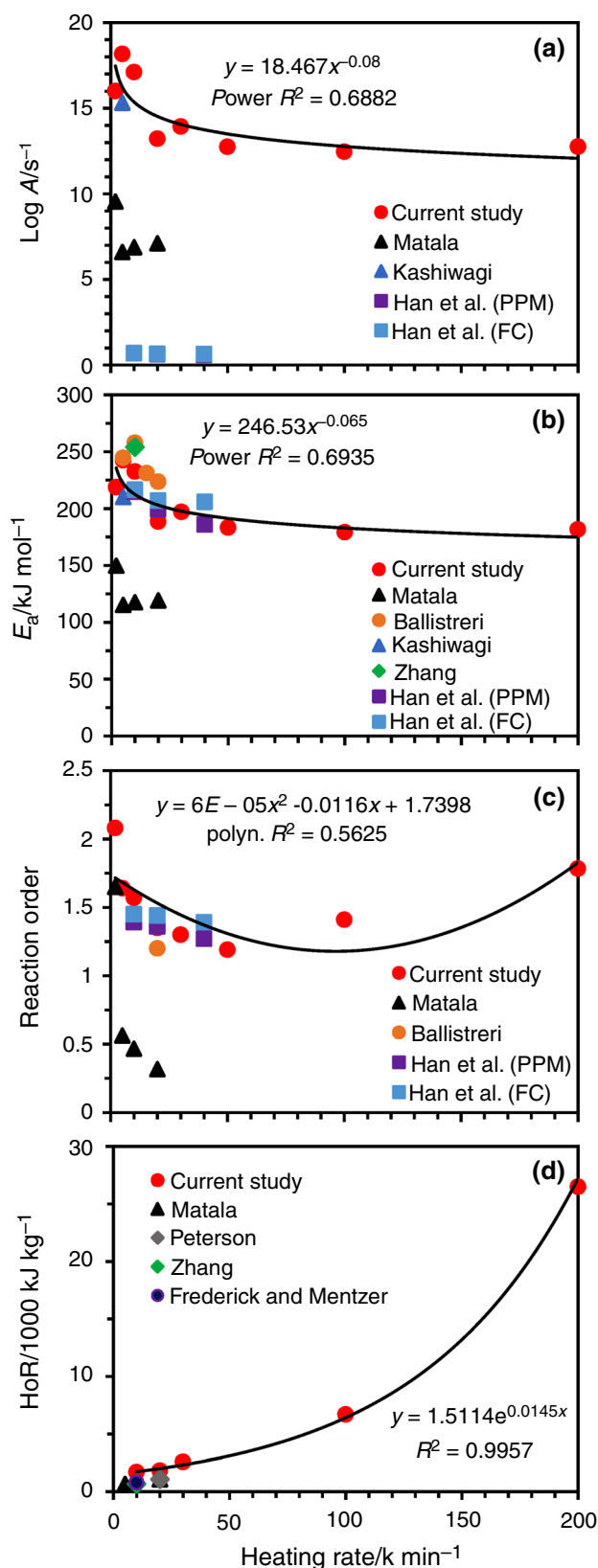


Fig. 3 PMMA kinetic parameters: **a** natural log of A ; **b** E_a ; **c** reaction order, n ; and **d** HoR as a function of heating rate

A values in the present study are close to those of Matala [27] and Kashiwagi et al. [33] at lower heating rates; however, the latter study was only conducted at a heating rate of 5 K min^{-1} . Most of these studies were conducted at heating rates between 0.5 and 40 K min^{-1} which would be considered relatively low, and given that these literature values at low heating rates compare well, it may be suggested that the values found in this study over the range of heating rates are reliable. To provide further evidence of reliability, Fig. 4 presents a comparison between the real data and that calculated from the derived kinetic triplets. In Fig. 4a, for the 5 K min^{-1} heating rate, the TG curves calculated from the triplets of Kashiwagi et al. [33], Matala [27] and the current study are compared with real data of the current study. Comparing the two TG curves of the current study, an excellent fit between the real data and that calculated from the triplet derived is observed. The results of the current study are also quite close to that calculated using the triplet of Kashiwagi et al. [33], and the difference may be attributed to the different formulation of PMMA and experimental equipment used. In Fig. 4b, for the 20 K min^{-1} heating rate, the real data from MTGA and PTGA match adequately with the TG curve calculated from one set of the derived kinetic triplet. Due to the

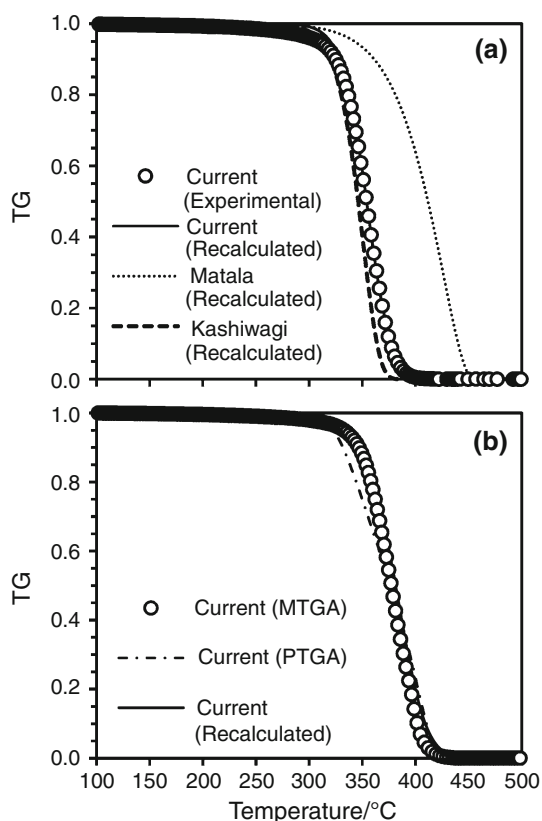


Fig. 4 Comparison between the real data and that calculated from the triplets derived: **a** 5 K min^{-1} and **b** 20 K min^{-1}

scarcity of reliable literature data obtained at higher heating rates (i.e. $50\text{--}200 \text{ K min}^{-1}$), the data from this study could not be comprehensively compared for PMMA at these rates.

In general, the kinetic parameters of PMMA show that the values of A and E_a decline as a function of heating rate. At lower heating rates, the chemical reaction is kinetically slow resulting in higher E_a values with the opposite occurring at higher heating rates [9]. It may be suggested that the E_a is controlled by the pyrolysis rate of the sample at the surface at higher heating rates, whereas at lower heating rates, bond breaking is the main contributor to the value of E_a [43]. Overall, the kinetic triplet is observed to change significantly with a variation in heating rates and it has been suggested that this is influenced by physical and chemical changes of materials [44]. As shown by the best-fit lines in Fig. 3, the implied relationship between $\log(A)$ and E_a with heating rate is empirically based on a power law, whereas for n , the relationship is more parabolic. In the equation presented in Fig. 3c, although the fitting of a quadratic polynomial ($R^2 = 0.56$) has been observed to be much better than a linear function ($R^2 = 0.0041$) with the selection of average value of n (1.54), a summary of the trends and qualitative correlations of the relationships all parameters PMMA with heating rate are presented in Table 1 which shows that all kinetic parameters decrease with an increasing heating rate.

Alternative pyrolysis parameters

Some fire models such as FDS [15] also offer an alternative method for determining the conversion rate using a combination of the DTG peak location, the peak value, and the pyrolysis range which is the approximate width of the DTG curve assuming the shape is triangular. Figure 5 shows these values obtained from the DTG curves as a function of heating rate. The regression analyses of all three parameters for PMMA show strong power trends for the reference temperature and reference reaction rate and a strong linear trend for the pyrolysis range. The values of other two parameters: v_s (the yield of solid residue) and $Y(0)$ (initial

Table 1 Summary of kinetic parameters and HoR trends with heating rate

Parameter	Trend	Strength
$\log(A)$	Power (decreasing)	Moderate ($R^2 = 0.69$)
E_a	Power (decreasing)	Moderate ($R^2 = 0.68$)
n	Parabolic (lower vertex)	Poor ($R^2 = 0.56$)
HoR	Exponential (increasing)	Strong ($R^2 = 1.0$)

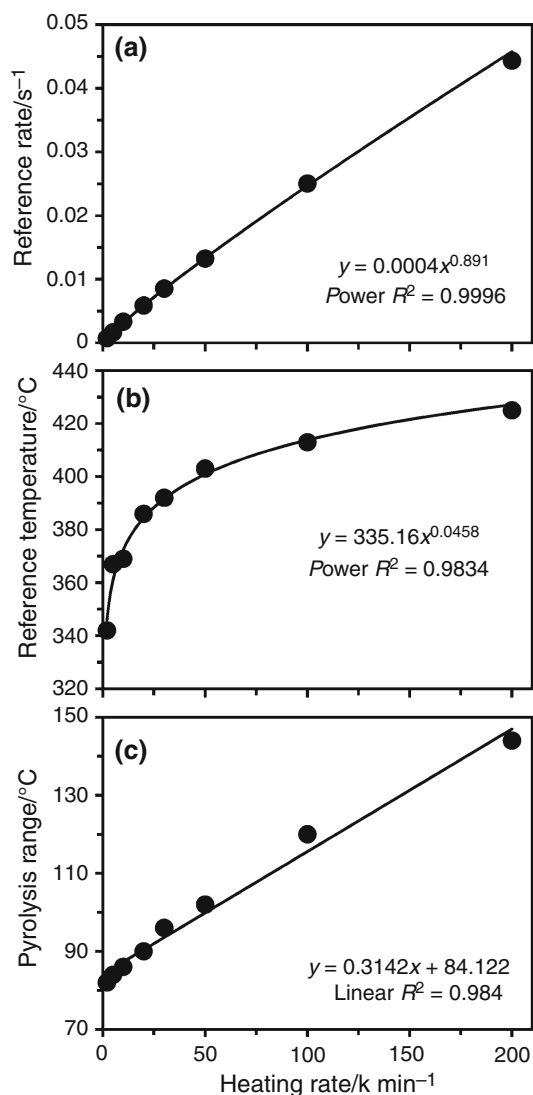


Fig. 5 Reference rate (a); reference temperature (b); and pyrolysis range (c) for PMMA as a function of heating rate

mass fraction) are 0 (zero) and 1, respectively, as expected from a non-charring polymer.

HoR of PMMA

The HoR values calculated based on the normalized enthalpy as a function of heating rate for PMMA are presented in Fig. 3d. Zhang [41] reported a HoR value of 687 kJ kg^{-1} measured at a heating rate of 10 K min^{-1} and Peterson et al. [45] obtained a HoR of 1080 kJ kg^{-1} at 20 K min^{-1} which are both lower than that in the current study. Frederick and Mentzer [46] obtained a HoR value of 804 kJ kg^{-1} at 10 K min^{-1} where this value is in between the values obtained by Zhang [41] and Peterson et al. [45]. An increasing trend of HoR value with respect to heating rate is observed, which was also observed for the thermal

decomposition of waste materials [35]. Haseli et al. [44] suggested that the external heating rate of the material is one of the primary reasons for HoR variations. For the data of the present study, regression analyses show that a very strong exponential relationship exists.

Characterization of combustion parameters

The HRR of all heat fluxes is shown in Fig. 6a where these curves represent the average value of the tested parameter. A quasi-steady burning was observed for all PMMA samples as described by Harper [47] for relatively thick sample of the non-charring polymer and a bubbling phenomenon occurred as a result of the breakdown of PMMA molecular bonds during the exposure of high temperature with the releasing gasses causing the bubbles [48]. Zeng et al. [49] suggested that the steady-state burning of PMMA may be due to the large thermal capacity of the material. A second peak in the HRR curve is observed at the end of the test, and this is also reported in a number of other studies [9, 48, 49]. Since PMMA is a non-charring polymer, it leaves little or no residue after burnout and this is in agreement with the findings of Luche et al. [24] and Spearpoint and Quintiere [50]. A greater heat exposure results in higher HRR, and this observation is consistent with the result obtained by Linteris et al. [51]. According to Shi and Chew [9], the HRR of non-charring polymers varies with heat flux due to the increment in pyrolysis rate as the heat flux increases and more heat is absorbed. The MLR as a function of time at different heat flux values is shown in Fig. 6b, and similar to the HRR, the MLR of PMMA increases with increasing heat flux and achieves a quasi-steady state after ignition.

The average CO yield is presented in Fig. 6c which shows it was released over a steady phase with a peak near the end of the test. Moreover, the CO yield is observed to increase with an increasing heat flux. The CO₂ yield is presented in Fig. 6d, and a steady state is observed with change in heat flux with the exception of 75 kW m^{-2} irradiance where a slightly decreasing trend with burning period is observed. Similar to the production of CO, it appears there is an incremental increase in the production of CO₂ with an increasing heat flux. The average CO yield at 50 kW m^{-2} irradiance is 0.009 kg kg^{-1} , and this is close to the value of $0.0098 \text{ kg kg}^{-1}$ found by Nelson and Jayakody [52]. Additionally, their reported value for CO₂ yield is 1.64 kg kg^{-1} , slightly lower than 2.091 kg kg^{-1} in the present study. The CO and CO₂ release and yield from combustible products is believed to be related to the heat release rate properties [53], and this may explain the similar trends observed in both parameters, although the CO₂ yield is observed to have less dependency on the HRR than the CO yield. As shown in Fig. 6e, the heat flux and hence

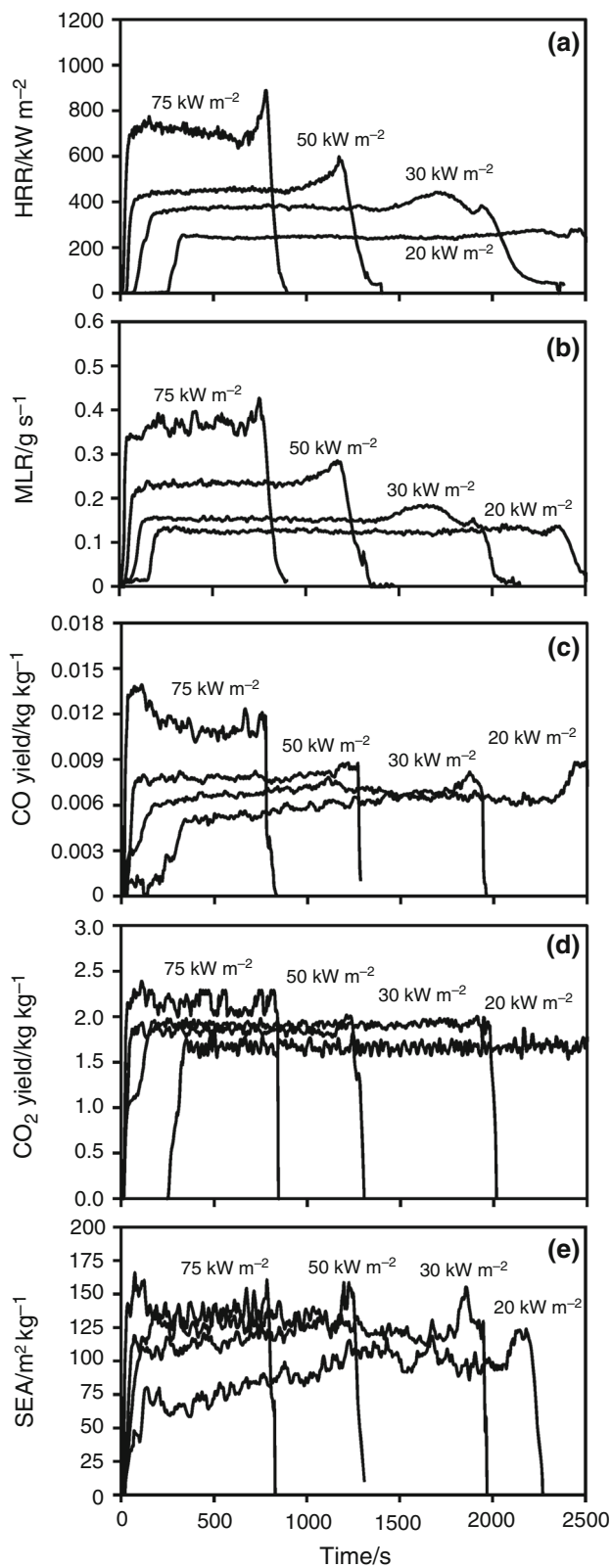


Fig. 6 Combustion parameters of PMMA at various heat fluxes: **a** average HRR; **b** average MLR; **c** average CO yield; **d** average CO₂ yield; and **e** specific extinction area

the HRR have little effect on the SEA which was relatively constant through the burning phase for all heat fluxes.

The cone calorimeter software provides average values of EHoC (or HRR/MLR), SEA, CO yield and CO₂ yield for 6 min after ignition. The soot yield is then derived from the SEA by division with a constant value of 8700 [54]. The average values of EHoC, CO yield and soot yield as functions of heat fluxes for PMMA are presented in Fig. 7. The average values of EHoC and CO₂ yield are $22.79 \pm 2.8 \text{ MJ kg}^{-1}$ and $1.97 \pm 0.2 \text{ kg kg}^{-1}$, respectively, with the value of EHoC reasonably close to the value of 24.0 MJ kg^{-1} obtained at 50 kW m^{-2} irradiance by Nelson and Jayakody [52]. Through regression analysis for the CO and soot yield of PMMA, empirical linear formulae as a function of irradiance were obtained and are shown in Fig. 7b, c.

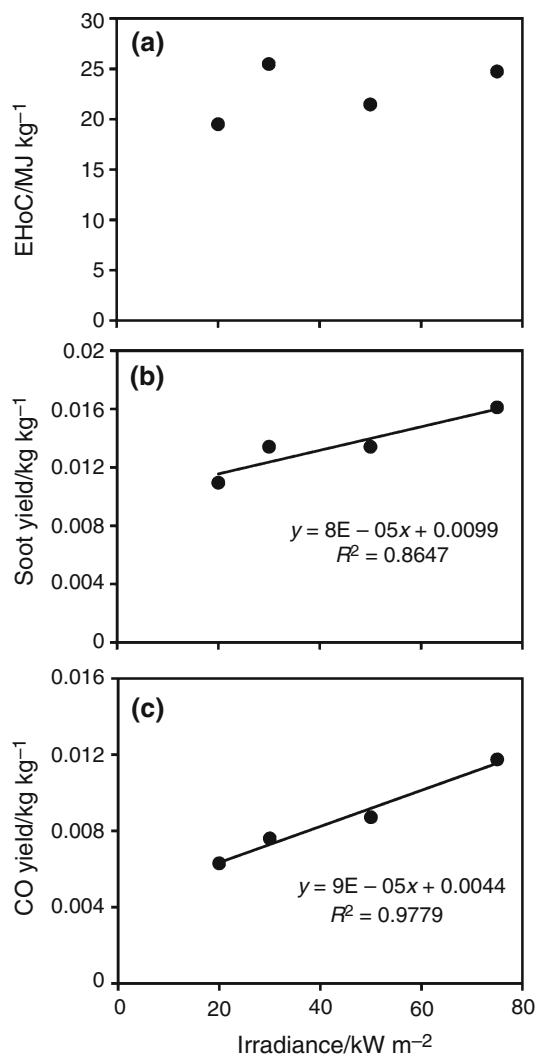


Fig. 7 Correlation of PMMA combustion parameters as a function of heat flux: **a** EHoC; **b** soot yield; and **c** CO yield

Characterization of thermo-physical parameters

The values of k for PMMA from the current study are presented in Fig. 8a along with comparative literature data. Although a sinusoidal pattern is observed, the k value does not significantly change with temperature, and the average value was $0.195 \pm 0.005 \text{ W m}^{-1} \text{ K}^{-1}$. Assael et al. [55] reported a similar finding for PMMA with a relatively stable value of k although only two temperatures were tested. The present study was performed over a wider temperature range between 30 and 100 °C at 10 °C increments, and as a result, significantly more thermal conductivity data were collected. Moreover, there are very little literature data available for thermal conductivities measured at temperatures greater than 80 °C and therefore comparisons could not be made with the some of the current data [56]. It is also important to note that it is not possible to measure the thermal conductivity of PMMA beyond 100 °C as the polymer undergoes phase change above this point and begins to melt [57]. This is an inherent limitation of the equipment used to perform this measurement due to the construction of the sensor. However, the average value from the current study can be used as an input into the conductive heat transfer calculation and in the pyrolysis simulation. Figure 8b presents the C_p of PMMA tested between 30 and 100 °C with comparative literature data from Assael et al.

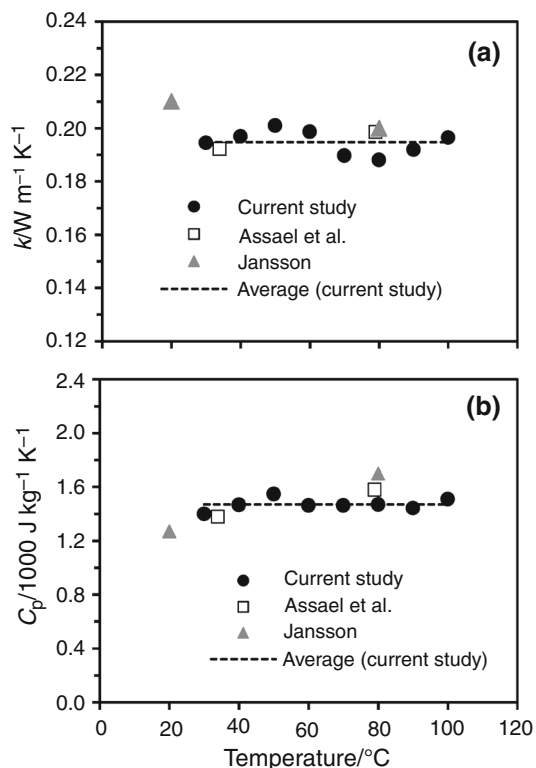


Fig. 8 PMMA thermal conductivity (a) and specific heat (b) as function of temperature

[55] and Jansson [56] also presented in the same figure. In the current study, the C_p values of PMMA range between 1300 and 1500 $\text{J kg}^{-1} \text{ K}^{-1}$ with an average value of $1471 \pm 597 \text{ J kg}^{-1} \text{ K}^{-1}$. The literature values are similar to this data, and although these examples only show limited data points, no trend of C_p with increasing temperature is observed.

Conclusions

A study to characterize the fire properties of PMMA for coupled pyrolysis and combustion simulation was conducted. Thermal analysis instrumentation including DSC and TGA was used at various heating rates to extract the relevant kinetic data. At the lower heating range, the kinetic data obtained for PMMA was in good agreement with literature values. However, significant variations of these values with respect to heating rate were observed and this may be due to its physical and chemical properties. The trends and relative fit of the relationships for each parameter of PMMA were evaluated, and it is clear that kinetic parameters show decreasing trends with respect to increasing heating rates with respect to A and E_a . For n , there was a moderate parabolic (lower vertex) trend. For the combustion parameters, no significant trend was observed for EHoC and this may be attributed to the absence of moisture and the subsequent lack of char formation. The thermal conductivity and specific heat of PMMA did not demonstrate any significant effect with changing in temperature. These parameters, in combination with other material specific data such as moisture content, can be used as input data to CFD-based fire models for the evaluation and modelling of the pyrolysis and combustion of PMMA and other similar materials.

Acknowledgements The authors wish to acknowledge the technical and financial assistance provided by Omnii Pty Ltd, Xtralis and Scientific Fire Services. The authors also acknowledge stimulating discussions with Dr. Yun Jiang of Xtralis. Ariza S. Abu-Bakar was a Ph.D. candidate at Victoria University funded by Universiti Sains Malaysia and currently employed by the same university.

References

- McGrattan K, et al. Fire dynamics simulator (version 6.2): user's guide. Gaithersburg: National Institute of Standard and Technology; 2015.
- Abu-Bakar AS, Moinuddin KAM. Effects of variation in heating rate, sample mass and nitrogen flow on chemical kinetics for pyrolysis. In: 18th Australasian fluid mechanics conference. Launceston, TAS; 2012.
- Font R, et al. Kinetics of pyrolysis and combustion of pine needles and cones. *J Anal Appl Pyrol.* 2009;85(1):276–86.

4. Gai C, Dong Y, Zhang T. The kinetic analysis of the pyrolysis of agricultural residue under non-isothermal conditions. *Bioresour Technol.* 2013;127:298–305.
5. Jiang Y. *Decomposition, ignition and flame spread on furnishing materials.* Melbourne: CESARE, Victoria University; 2006.
6. Matala A, Hostikka S, Mangs J. Estimation of pyrolysis model parameters for solid materials using thermogravimetric data. *Fire Saf Sci.* 2008;9:1213–23.
7. Starink MJ, Gregson PJ. A quantitative interpretation of DSC experiments on quenched and aged SiCp reinforced 8090 alloys. *Scr Metall Mater.* 1995;33(6):893–900.
8. American Society for Testing and Materials. ASTM 1354-04a, standard test method for heat and visible smoke release rates for materials and products using an oxygen consumption calorimeter. West Conshohocken, PA: ASTM International; 2004. www.astm.org. Accessed 03 Feb 2010.
9. Shi L, Chew MYL. A review of fire processes modeling of combustible materials under external heat flux. *Fuel.* 2013;106:30–50.
10. Xu Q, et al. Discuss the heat release capacity of polymer derived from microscale combustion calorimeter. *J Therm Anal Calorim.* 2018;133(1):649–57.
11. Xu Q, et al. A PMMA flammability analysis using the MCC. *J Therm Anal Calorim.* 2016;126(3):1831–40.
12. Pau DSW. A comparative study on combustion behaviours of polyurethane foams with numerical simulations using pyrolysis models. Christchurch: Civil and Natural Resources Engineering, University of Canterbury; 2013.
13. Viswanath SG, Gupta MC. Estimation of nonisothermal kinetic parameters from a TG curve by the methods of overdetermined system and inflection point. *Thermochim Acta.* 1996;285(2):259–67.
14. Wadhvani R, et al. Kinetics of pyrolysis of litter materials from pine and eucalyptus forests. *J Therm Anal Calorim.* 2017;130(3):2035–46.
15. McGrattan K, Forney G. *Fire dynamics simulator (version 4) user's guide.* 4th ed. Washington: US Government Printing Office; 2006.
16. Gustafsson SE. Transient plane source techniques for thermal conductivity and thermal diffusivity measurements of solid materials. *Rev Sci Instrum.* 1991;62(3):797–804.
17. Sibulkin M. Heat of gasification for pyrolysis of charring materials. In: *Proceedings of the first international symposium on fire safety science.* Boca Raton: CRC Press; 1986.
18. Kodur VKR, Harmathy TZ. Properties of building materials. In: DiNenno PJ, editor. *SFPE handbook of fire protection engineering.* 3rd ed. Berlin: Springer; 2002. p. 155–81.
19. Huffman R, Pan W-P. Combining DSC and TG data for measuring heats of reaction. *Thermochim Acta.* 1990;166:251–65.
20. Rath J, et al. Heat of wood pyrolysis. *Fuel.* 2003;82(1):81–91.
21. Abu-Bakar AS. Characterization of fire properties for coupled pyrolysis and combustion simulation and their optimised use. Melbourne: College of Engineering and Science, Victoria University; 2015.
22. Fang MX, et al. Kinetic study on pyrolysis and combustion of wood under different oxygen concentrations by using TG-FTIR analysis. *J Anal Appl Pyrol.* 2006;77(1):22–7.
23. Gao N, et al. TG-FTIR and Py-GC/MS analysis on pyrolysis and combustion of pine sawdust. *J Anal Appl Pyrol.* 2013;100:26–32.
24. Luche J, et al. Characterization of thermal properties and analysis of combustion behavior of PMMA in a cone calorimeter. *Fire Saf J.* 2011;46(7):451–61.
25. American Society for Testing and Materials. ASTM E2160-04 standard test method for heat of reaction of thermally reactive materials by differential scanning calorimetry. West Conshohocken, PA: ASTM International; 2004. www.astm.org. Accessed 03 Feb 2010.
26. Hostikka S. 2012. (Personal Communication)
27. Matala A. Estimation of solid phase reaction parameters for fire simulation. Espoo: Faculty of Information and Natural Sciences, Helsinki University of Technology; 2008.
28. Li K-Y, et al. Pyrolysis of medium-density fiberboard: optimized search for kinetics scheme and parameters via a genetic algorithm driven by Kissinger's method. *Energy Fuels.* 2014;28(9):6130–9.
29. Zhang Z et al. Effect of temperature and heating rate in pyrolysis on the yield, structure and oxidation reactivity of pine sawdust biochar. In: *Chemeca 2013: challenging tomorrow.* Barton, ACT: Engineers Australia; 2013. p. 863–9.
30. Kim S-S, et al. Pyrolysis kinetics and decomposition characteristics of pine trees. *Bioresour Technol.* 2010;101(24):9797–802.
31. Wang G, et al. TG study on pyrolysis of biomass and its three components under syngas. *Fuel.* 2008;87(4):552–8.
32. Mui ELK, et al. Kinetic study on bamboo pyrolysis. *Ind Eng Chem Res.* 2008;47(15):5710–22.
33. Kashiwagi T, Inaba A, Brown JE. Differences in PMMA degradation characteristics and their effects on its fire properties. *Fire Saf Sci.* 1986;1:483–93.
34. Kissinger HE. Variation of peak temperature with heating rate in differential thermal analysis. *J Res Nat Bur Stand.* 1956;57(4):217–21.
35. Missoum A, Gupta AK, Chen J. Global kinetics of the thermal decomposition of waste materials. In: *Thirty-second intersociety energy conversion engineering conference (IECEC-97).* Honolulu, HI; 1997. p. 636–41.
36. Quan C, Li A, Gao N. Thermogravimetric analysis and kinetic study on large particles of printed circuit board wastes. *Waste Manag.* 2009;29(8):2353–60.
37. Milosavljevic I, Oja V, Suuberg EM. Thermal effects in cellulose pyrolysis: relationship to char formation processes. *Ind Eng Chem Res.* 1996;35(3):653–62.
38. Lautenberger C, Rein G, Fernandez-Pello C. The application of a genetic algorithm to estimate material properties for fire modeling from bench-scale fire test data. *Fire Saf J.* 2006;41(3):204–14.
39. Opfermann J. Kinetic analysis using multivariate non-linear regression. I. Basic concepts. *J Therm Anal Calorim.* 2000;60(2):641–58.
40. Ballistreri A, Montaudo G, Puglisi C. Reliability of the volatilization method for determination of the activation energy in the thermal decomposition of polymers. *J Therm Anal.* 1984;29(2):237–41.
41. Zhang H. *Fire-safe polymers and polymer composites.* Washington: Federal Aviation Administration, Office of Aviation Research; 2003.
42. Han TU, et al. Pyrolysis kinetic analysis of poly(methyl methacrylate) using evolved gas analysis-mass spectrometry. *Korean J Chem Eng.* 2017;34(4):1214–21.
43. Ang HG, Pisharath S. *Energetic polymers.* New York: Wiley; 2012.
44. Haseli Y, van Oijen JA, de Goey LPH. Modeling biomass particle pyrolysis with temperature-dependent heat of reactions. *J Anal Appl Pyrol.* 2011;90(2):140–54.
45. Peterson JD, Vyazovkin S, Wight CA. Kinetic study of stabilizing effect of oxygen on thermal degradation of poly(methyl methacrylate). *J Phys Chem B.* 1999;103(38):8087–92.
46. Frederick WJ, Mentzer CC. Determination of heats of volatilization for polymers by differential scanning calorimetry. *J Appl Polym Sci.* 1975;19(7):1799–804.
47. Harper CA. *Handbook of building materials for fire protection.* New York: McGraw-Hill; 2004.
48. Steinhaus T. Evaluation of the thermophysical properties of poly(methylmethacrylate): a reference material for the

- development of a flammability test for micro-gravity environments. College Park: Department of Fire Protection Engineering, The University of Maryland; 1999.
49. Zeng WR, Li SF, Chow WK. Preliminary studies on burning behavior of polymethylmethacrylate (PMMA). *J Fire Sci.* 2002;20(4):297–317.
 50. Spearpoint MJ, Quintiere JG. Predicting the piloted ignition of wood in the cone calorimeter using an integral model: effect of species, grain orientation and heat flux. *Fire Saf J.* 2001;36(4):391–415.
 51. Linteris GT et al. Modeling solid sample burning. In: Eighth international symposium international association for fire safety science (IAFSS). Boston, MA; 2005.
 52. Nelson GL, Jayakody C. Flame retardant polyurethane. In: Flame retardant polymers: electrical/electronic applications. Boca Raton: CRC Press; 1998. p. 1–28.
 53. Babrauskas V, Peacock RD. Heat release rate: the single most important variable in fire hazard. *Fire Saf J.* 1992;18(3):255–72.
 54. Mulholland GW, Croarkin C. Specific extinction coefficient of flame generated smoke. *Fire Mater.* 2000;24(5):227–30.
 55. Assael MJ, et al. Thermal conductivity of polymethyl methacrylate (PMMA) and borosilicate crown glass BK7. *Int J Thermophys.* 2005;26(5):1595–605.
 56. Jansson R. Measurement of thermal properties at elevated temperatures: Brandforsk project 328-031. SP report 2004:46, 2004.
 57. Smith WF, Hashemi J. Polymeric materials. In: Foundations of materials science and engineering. New York: McGraw-Hill; 2006. p. 515–6.